

An Artificial SEI Layer Based on an Inorganic Coordination Polymer with Self-Healing Ability for Long-Lived Rechargeable Lithium-Metal Batteries

Witali Beichel,^{*[a]} Julian Skrotzki,^[a, b] Petra Klose,^[b, c] Christian Njel,^[d] Burkhard Butschke,^[b] Stephan Burger,^[b, c] Lili Liu,^[e] Ralf Thomann,^[c, f] Yi Thomann,^[c, f] Daniel Biro,^[g] Simon Thiele,^[h, i] and Ingo Krossing^{*[b, c, f]}

Upon immersion of a lithium (Li) anode into a diluted 0.05 to 0.20 M dimethoxyethane-solution of the phosphoric acid derivative ($\text{CF}_3\text{CH}_2\text{O}_2\text{P}(\text{O})\text{OH}$) (HBFEP), an artificial solid electrolyte interphase (SEI) is generated on the Li-metal surface. Hence, HBFEP reacts on the surface to the corresponding Li salt (LiBFEP), which is a Li-ion conducting inorganic coordination polymer. This film exhibits – due to the reversibly breaking ionic bonds – self-healing ability upon cycling-induced volume expansion of Li. The presence of LiBFEP as the major component in the artificial SEI is proven by ATR-IR and XPS

measurements. SEM characterization of HBFEP-treated Li samples reveals porous layers on top of the Li surface with at least 3 μm thickness. Li–Li symmetrical cells with HBFEP-modified Li electrodes show a three- to almost fourfold cycle-lifetime increase at 0.1 mA cm^{-2} in a demanding model electrolyte that facilitates fast battery failure (1 M LiOTf in TEGDME). Hence, the LiBFEP-enriched layer apparently acts as a Li-ion conducting protection barrier between Li and the electrolyte, enhancing the rechargeability of Li electrodes.

Introduction

Lithium (Li) metal has been identified as a promising anode material for future battery cell concepts due to its high theoretical volumetric as well as gravimetric capacity. Investigations on rechargeable battery systems with Li as the anode are manifold and are generally denoted as Li-metal batteries (LMBs). Either combined with a transition-metal oxide (TMO) or a conversion-type cathode (S, O_2) and a liquid, semi-solid or solid electrolyte, LMBs have a huge potential to overcome the

energy storage limits of current Li-ion batteries (LIBs).^[1] To date, specific energies and energy densities of up to 500 Wh kg⁻¹ and 1200 Wh L⁻¹ have been achieved for LMBs with TMO cathodes^[2–7] on the pouchbag cell level (*cf.* 180 Wh kg⁻¹ and 450 Wh L⁻¹ for state-of-the-art LIBs).^[8] Among LMBs with conversion-type electrodes, gravimetric energies of 400 Wh kg⁻¹ for the Li–S battery of Oxis Energy have been realized as well.^[9] Despite these achievements, the cycle life of LMBs is usually limited to up to several hundred cycles.^[2–7,9] Therefore, continuous efforts are necessary to develop and

- [a] Dr. W. Beichel, J. Skrotzki
Chair of Solar Energy Systems, Department of Sustainable Systems Engineering (INATECH)
University of Freiburg
Emmy-Noether-Strasse 2, 79110 Freiburg im Breisgau, Germany
E-mail: witali.beichel@inatech.uni-freiburg.de
- [b] J. Skrotzki, P. Klose, Dr. B. Butschke, S. Burger, Prof. Dr. I. Krossing
Institute for Inorganic and Analytical Chemistry
University of Freiburg
Albertstr. 21, 79104 Freiburg im Breisgau, Germany
E-mail: ingo.krossing@ac.uni-freiburg.de
- [c] P. Klose, S. Burger, Dr. R. Thomann, Dr. Y. Thomann, Prof. Dr. I. Krossing
Freiburg Materials Research Center (FMF)
University of Freiburg
Stefan-Meier-Str. 21, 79104 Freiburg im Breisgau, Germany
- [d] Dr. C. Njel
Institute for Applied Materials (IAM) and Karlsruhe Nano Micro Facility (KNMF)
Karlsruhe Institute of Technology (KIT)
Hermann-von-Helmholtz-Platz 1, 76344 Eggenstein-Leopoldshafen, Germany
- [e] Prof. Dr. L. Liu
School of Energy Science and Engineering
Nanjing Tech University
Jiangsu Province, Nanjing 211816, China

[f] Dr. R. Thomann, Dr. Y. Thomann, Prof. Dr. I. Krossing
Freiburg Center for Interactive Materials and Bioinspired Technologies (FIT)
University of Freiburg
Georges-Koehler-Allee 105, 79110 Freiburg im Breisgau, Germany

[g] Dr. D. Biro
Department Electrical Energy Storage
Fraunhofer Institute for Solar Energy Systems ISE
Heidenhofstraße 2, 79110 Freiburg im Breisgau, Germany

[h] Prof. Dr. S. Thiele
Helmholtz Institute Erlangen-Nürnberg for Renewable Energy (IEK-11)
Forschungszentrum Jülich GmbH
Egerlandstr. 3, 91058 Erlangen, Germany

[i] Prof. Dr. S. Thiele
Department of Chemical and Biological Engineering
Friedrich-Alexander-Universität Erlangen-Nürnberg
Egerlandstr. 3, 91058 Erlangen, Germany

 Supporting information for this article is available on the WWW under <https://doi.org/10.1002/batt.202100347>

 © 2021 The Authors. *Batteries & Supercaps* published by Wiley-VCH GmbH. This is an open access article under the terms of the Creative Commons Attribution Non-Commercial NoDerivs License, which permits use and distribution in any medium, provided the original work is properly cited, the use is non-commercial and no modifications or adaptations are made.

improve approaches for the realization of commercially relevant, durable, cheap, and high performing LMBs.

Irrespective of the technology, the use of Li metal as an anode poses a huge challenge for the realization of durable LMBs. In contrast to LIBs, stable solid-electrolyte interphases (SEI) are absent during operation. Continuous electrolyte decomposition, low coulombic efficiencies and the formation of dendrites prevent a long-term and stable cycling behavior of LMBs.^[10,11] Various approaches to stabilize the Li metal anode exist, which can be categorized into a) electrolyte modification, b) ex-situ application of protective layers, c) mechanical modification, d) separator modification, e) improved anode structure design, and f) others.^[12–15] Among these approaches, the use of protective layers – also known as artificial SEI – is quite promising with respect to practical large-scale applications.^[16–19]

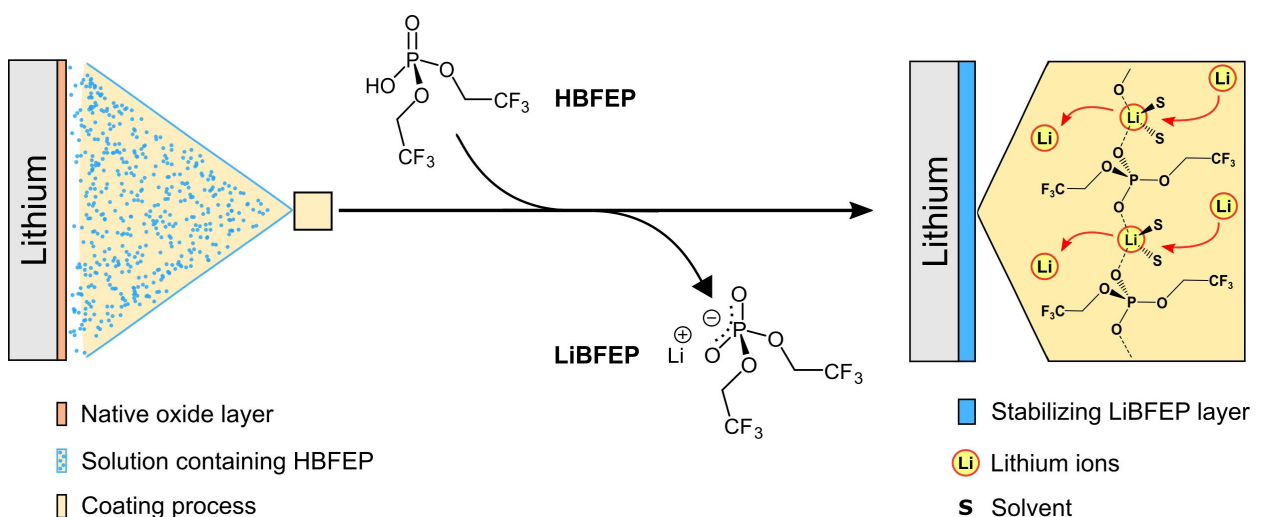
In commercial LIBs, the SEI is formed *in situ* from electrolyte constituents during the first charge-discharge formation-cycles. With Li metal, a rather unstable SEI is formed upon the first contact with the standard electrolyte and in subsequent charge-discharge cycles.^[20,21] In contrast, the artificial SEI approach allows for the ex-situ deposition of protective layers on Li prior to battery operation. Hence, with the artificial SEI approach it is the possible to control and regulate SEI composition by a knowledge-driven choice of reagents and deposition method.^[18,19] Hitherto, numerous protective layer types were applied to Li-metal anodes via various deposition methods.^[11,16–19] The materials range from inorganic materials, polymers, inorganic-organic hybrids and molecular compounds, while the deposition methods encompass atomic or molecular layer deposition, solid gas reaction or wet chemical coating.^[11,17,19] So far, Li has been modified with gases,^[22] neat liquids,^[23] and various solutions.^[24] All pre-treatments mentioned led to improved Li-metal cycling in model test cells on the laboratory scale.

Here *bis*(1,1,1-trifluoroethyl)-phosphoric acid $[(CF_3CH_2O)_2PO(OH)]$ (HBFEP) is used as a reagent to generate an

artificial SEI on Li metal (Scheme 1). The synthesis and characterization of HBFEP as well as of the corresponding Li-salt LiBFEP were reported by us.^[25] Upon contact with carbonate-based liquid organic electrolytes (e.g., 1 M Li[PF₆] in EC/DMC), LiBFEP forms gels. Interestingly, the ionic conductivities of these highly viscous gels are similar to pure liquid electrolytes (6–10 mS cm⁻¹).^[25] Furthermore, LiBFEP exhibits a long-term compatibility with Graphite–NMC111 full cells^[25] and has been applied as a high-voltage electrolyte-additive in Graphite–LNMO full cells.^[26] Since HBFEP is a hydrofluorocarbon-substituted phosphoric-acid derivate, it is able to react with the basic surface species on Li and even with Li directly. This mode of action can be considered as a cleaning step, accompanied by the deposition of LiBFEP as a reaction product.

In its crystalline form, HBFEP forms a 1D coordination polymer with the central H⁺ bridging neighboring [BFEP]⁻ anions. We suggested that gelled LiBFEP also forms a coordination polymer (Scheme 1: inset on the right side) to account for the peculiar gelling properties of LiBFEP in organic carbonate solvents.^[25] Due to the presence of ionic bonds, we propose that the LiBFEP coordination polymer forms an SEI and exhibits self-healing or self-adaptive properties. The term “self-healing” is used here in the sense of Wang and Urban^[27] as “the capability to recover from physical damage”. Self-adaption is understood by the present authors as the ability of accommodation of mechanical deformations.^[28]

Thus, the Brønsted acid HBFEP shall first act as a chemical cleaning agent. Second, the LiBFEP reaction product is a Li-ion conducting coordination polymer.^[25] Together they have the potential to act as an artificial SEI with adaptive and self-healing properties. To the best of our knowledge, no report of a single inorganic agent combining these two aspects appeared yet. Tang et al. used a naphthalene-containing solution as a chemical polisher only.^[29] Several researchers reported on acidic treatments of Li with HIO₃,^[30] H₃PO₄,^[31] polyphosphoric acid,^[31] and polyacrylic acid.^[32] Self-healing or



Scheme 1. Simplified scheme demonstrating the mode of operation using HBFEP as deposition reagent. Upon reaction with the native oxide layer, LiBFEP is formed. The latter acts as a Li-ion conducting protective artificial SEI layer prolonging the Li-metal anode's lifetime.

self-adapting properties of artificial SEI layers were reported as well.^[28,32–34]

Herein, we present the results of a proof-of-concept study as part of our ongoing work towards practical rechargeable LMBs: First the Li-metal surface is modified by HBFEP by a simple immersion process. In the next step, the chemical compositions and morphologies of the pristine and the modified Li-metal surfaces are analyzed in detail by ATR-IR, XPS and SEM measurements. Afterwards, the impact of such a surface treatment on the electrochemical performance in symmetrical Li–Li model test cells is presented. Finally, a possible mode of action of LiBFEP as an artificial SEI is proposed.

Results and Discussion

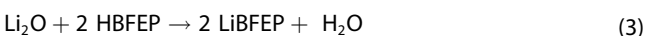
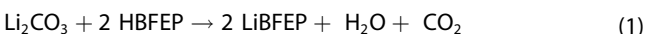
Chemical pretreatment

Li-metal discs were modified with HBFEP by a simple immersion process. The discs were put into a solution of HBFEP in 1,2-dimethoxyethane (DME) and stirred for a certain time. Afterwards, the solution was decanted, and the Li discs were dried in a glovebox. DME was selected as the solvent of choice since it dissolves HBFEP and evaporates rather quickly. Furthermore, DME is known to react with Li only slowly,^[35] and it might therefore be considered as an inert solvent in the present context. Consequently, we assign any changes in the physico- and electrochemical properties of the modified Li-discs to the presence HBFEP and its reaction products.

The chemical attachment of LiBFEP to the Li-metal surface as a protective layer deserves additional considerations. Commercially obtained Li-metal foils and discs exhibit native oxide-surface films with LiOH, Li₂O, Li₂CO₃ and hydrocarbons as the typical constituents.^[36] Such a basic surface film will react with the Brønsted acid HBFEP in an acid-base reaction. In the simplest case, HBFEP reacts stoichiometrically with the inorganic compounds according to Equations (1)–(3). The full or partial removal of the native oxide layer qualifies the compound HBFEP as a chemical cleaning agent. Once the native oxide layer has been consumed, excess HBFEP reacts with elemental Li according to Equation (4).

The water resulting from Equations (1)–(3) will either be released into the gas phase, removed with the DME solvent, or react with the subjacent Li and Li₂O according to Equations (5)–(7). Similarly, the evolving hydrogen [Eqs. (4), (6) and (7)] will escape as a gas or react to a minor extent with Li to form LiH. Finally, CO₂ from Equation (1) or as a contaminant from the ambient atmosphere will react with either Li₂O or LiOH [Eqs. (9) and (10)]. As a consequence of all these processes, the complete absence of inorganic layers or domains in the newly formed SEI is unlikely. Several of the mentioned reactions might even occur simultaneously. Although the direct reaction of HBFEP with Li might be hindered by the presence of blocking inorganic phases, LiBFEP can be formed at least via Equations (1)–(3) and deposit on the outer Li surface. Thus, in general and even without the exact knowledge of the course of

the reactions in Equations (1)–(10), the coverage of the Li surface by LiBFEP can be reasonably well expected (Scheme 1).



ATR-IR

ATR-IR spectroscopy is a very fast and straightforward characterization technique. Its penetration depth is in the μm range and is considered here as a bulk analysis of the modified Li surface. Therefore, it was used to monitor changes of the Li-metal surface after its modification and in order to get clues about the possible course of the reactions in Equations (1)–(4). Hence, Li discs were stirred for four minutes in DME-solutions of HBFEP with concentrations of 0.05, 0.10, 0.15 and 0.20 mol L⁻¹. The ATR-IR spectra of the modified Li discs were recorded afterwards and compared in Figure 1(b) to reference spectra, i.e., pristine Li (pLi), Li treated with DME only (DME–Li), and powdered LiBFEP (LiBFEP).^[25] The corresponding modified samples are designated as 0.05-HBFEP, 0.10-HBFEP, 0.15-HBFEP and 0.20-HBFEP. Overall, an increase of the modes characteristic for LiBFEP is visible between 1500–850 cm⁻¹ with increasing HBFEP concentration (Figure 1a). The spectra for the Li discs treated with 0.15 and 0.20 M HBFEP solutions even resemble those of powdered LiBFEP, i.e., bulk LiBFEP has been formed on the Li surface.

In order to resolve the peculiar features of the differently treated samples, selected spectra are shown in Figure 1(b) along with the most significant band assignments. The numerical values of all signals and their assignments are compiled in Table S-1 in the Supporting Information.

The pristine Li surface in Figure 1(b) exhibits intense bands between 2854 and 2954 cm⁻¹, characteristic for aliphatic C–H stretching vibrations.^[37] These features most probably stem from long-chain hydrocarbons, e.g., mineral oil, either used as

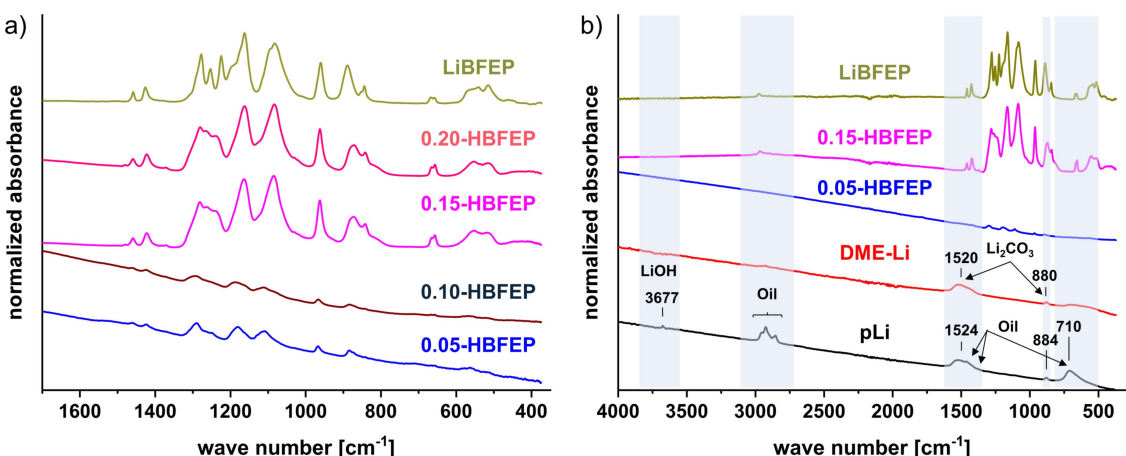


Figure 1. ATR-IR spectra of HBFEP modified Li discs that were stirred for four minutes in DME-solutions of HBFEP with concentrations of 0.05, 0.10, 0.15 and 0.20 mol L⁻¹ a) as a function of concentration and b) in comparison to reference spectra of pLi, DME-Li and powdered LiBFEP.

storage medium for Li or as a constituent of lubricants in the manufacturing process of the Li foils. The corresponding signals of the CH₂ bending vibrations are visible as shoulders at 1467, 1378 and at 710 cm⁻¹.^[37] The broad peak at 1520/1524 cm⁻¹ and the single sharp one at 880/884 cm⁻¹ are characteristic for the C–O stretching vibrations of Li₂CO₃.^[38]

The broad signal at 710 cm⁻¹ might contain contributions from additional inorganic species like Li₂O, LiOH and Li₃N.^[39] The sharp peak at 3675 cm⁻¹ corresponds to the O–H stretching vibration of LiOH.^[38] All these compounds (LiOH, Li₂O, Li₂CO₃ and hydrocarbons) are typical constituents of the native oxide film of pristine Li.^[36,38]

The treatment of Li with DME results in an almost disappearance of the aliphatic C–H vibrations and of the sharp LiOH band (Figure 1b). Additional signatures related to the possible decomposition of DME on Li were not observed.^[35] Volatile DME presumably evaporates without significant decomposition. Application of a 0.05 M HBFEP-solution to Li leads (almost) to the disappearance of all bands characteristic for the native oxide layer (Figure 1b). At the same time, bands characteristic for the [BFEP]⁻ anion (1500–850 cm⁻¹) appear. The enlarged spectrum in Figure 1(a) and the comparison with the numerical values in Table S-1 show that the treatment with 0.05 M HBFEP produces the main signatures of LiBFEP, however, with lower intensities and slight shifts compared to powdered LiBFEP. With increasing HBFEP concentration, also the signal intensities assigned to LiBFEP grow. Yet, the disappearance of the native oxide layer and formation of bands assigned to LiBFEP on the Li-metal surface even after treatment at low HBFEP concentrations suggest the formation of LiBFEP via Equations (1)–(3). From these explorative ATR-IR measurements an upper and lower HBFEP-concentration limit for the Li-disc treatment was suggested: LiBFEP formation can already be observed, when the four minutes treatment is conducted with 0.05 M solutions, while the saturation of the Li-metal surface with LiBFEP seems to start at a concentration of 0.15 M HBFEP in DME. Consequently, these two concentrations were selected for the further characterization.

XPS

While ATR-IR was used as a qualitative monitoring tool for the bulk composition of the layer, XPS was chosen to probe the outer surface. The C 1s, O 1s, P 2p, and F 1s XPS spectra of powdered LiBFEP, pLi, DME–Li, as well as of Li treated with 0.05 M and 0.15 M HBFEP in DME are shown in Figure 2. In Figure S-1, survey and Li 1s spectra for all samples are provided as well. The C 1s spectra (Figure 2a) comprise one component located at 285.0 eV, which is characteristic for C–C/C–H bonds. The spectrum of pLi displays components centered at 286.5, 289.0, and 290.2 eV, attributed to C–O, O–C=O, and Li₂CO₃ as always detected on the surface of fresh Li-metal electrodes.^[40,41] After HBFEP treatment, two new peaks appear. The peak at 293.5 eV corresponds to a CF₃ environment,^[42] while the peak at 288.6 eV is attributed to the mixture of O–C=O/P–O–C components. The latter feature constitutes the major contribution to the signal and is characteristic for the [BFEP]⁻ anion. From now on, we attribute XPS signals characteristic for the [BFEP]⁻ anion to LiBFEP directly. O 1s spectra show all oxygenated species present at the surface. On pLi and DME–Li samples, the two main peaks at 531.2 and 531.9 eV correspond to LiOH and a mixture of C=O/Li₂CO₃. Together with the weak peak at 533.9 eV (C–O environment) these peaks are signatures of the native oxide layer.^[36,41] The HBFEP treatment led to the appearance of three additional components, i.e., O²⁻ anions from Li₂O (528.5 eV), a mixture of C–O/P=O containing components (532.6 eV), and a C–O environment of the CF₃–CH₂–O groups of LiBFEP (534.3 eV). Phosphorus and fluorine were detected only on the surface of LiBFEP powder and for HBFEP-treated samples. The P 2p spectra were fitted with 2p_{3/2}–2p_{1/2} doublets separated by 0.9 eV with a 2/1-intensity ratio due to spin-orbit coupling. The doublet with the P 2p_{3/2} component at 135.2 eV is the signal of the C–O–P=O environment from LiBFEP. The F 1s spectra display two components, one located at 685.1 eV indicating the presence of LiF^[41] and one located around 689.0 eV indicating the presence of C–F bonds due to the CF₃ groups of LiBFEP. The LiF

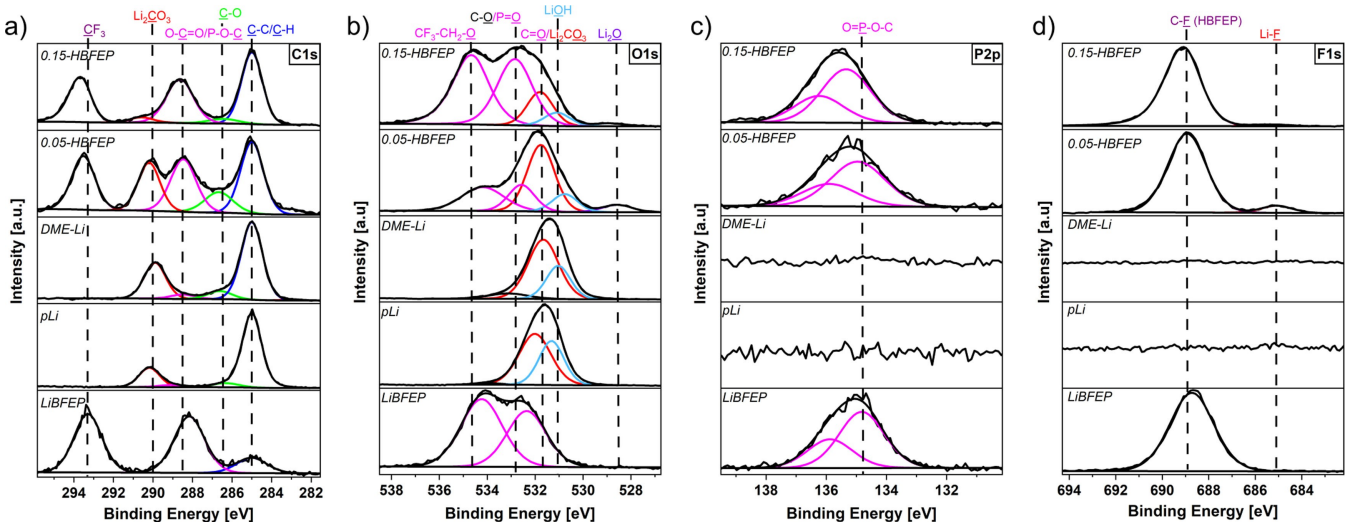


Figure 2. C 1s, O 1s, P 2p and F 1s XPS spectra of LiBFEP powder, of Li electrodes before (pLi) and after treatment (DME–Li, 0.05-HBFEP and 0.15-HBFEP).

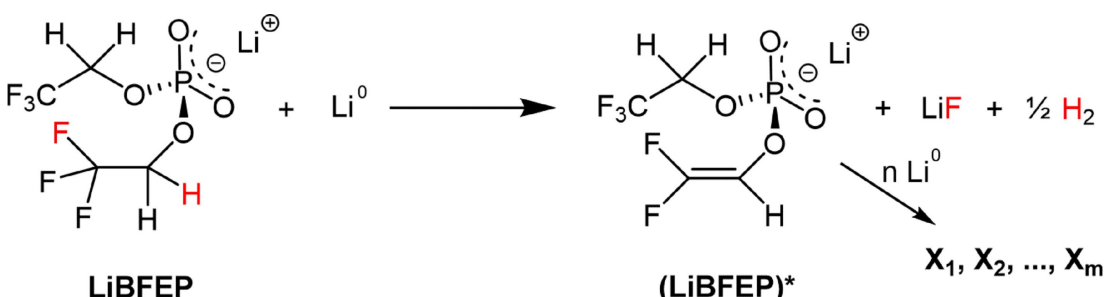
content on the surface of the 0.05-HBFEP is higher than that on the 0.15-HBFEP sample (Figure 2d). In the latter sample, the signal for LiF – although low in intensity – still contributes to the overall fit of the F 1s spectrum. Hence, the presence of LiF most probably stems from a partial decomposition of LiBFEP on the Li-metal surface via a reductive elimination mechanism as shown in Scheme 2.

C–F-bond cleavage under reductive conditions is well known for the $[\text{N}(\text{SO}_2\text{CF}_3)_2]^-$ anion^[43] and can be well adopted here. The product (LiBFEP)* might undergo additional decomposition pathways, e.g., reductive polymerization. The absence of additional distinct XPS- (or ATR-IR-) signals of decomposition products can be explained by their chemical similarity to the $[\text{BFEP}]^-$ skeleton. The proposed decomposition sequence suggests that a direct contact between the BFEP skeleton and Li has taken place before. From those considerations, the occurrence of direct reaction between HBFEP and Li [Equation (4)] is probable.

It is noteworthy, that the components of the initial native oxide layer are still observed. This fact might indicate the formation of inorganic phases in the course of the acidic treatment, [see Equations (5)–(7)]. Alternatively, it might simply be due to an incomplete conversion according to Equations (1)–(3).

To further analyze concentration effects of 0.05 vs. 0.15 M HBFEP solutions on the deposition process, we calculated the Li-surface species-distribution for all investigated samples. Representative orienting results are shown in Figure 3. Hence, the XPS analyses of the pLi and DME–Li samples reveal that the surface composition is dominated by Li_2CO_3 and LiOH (around 60%). Within the HBFEP-treated samples, the amount of LiBFEP increases from 38% (0.05-HBFEP) to 65% (0.15-HBFEP). At the same time, the total amount of Li_2CO_3 and LiOH decreased from 61% (pLi) to 30% (0.05-HBFEP) and even 7% (0.15-HBFEP). Furthermore, additional signals assigned to Li_2O are visible. The currently accepted model for the native oxide layer on Li bases on an inner Li_2O layer with thicknesses of 1–10 nm and an outer $\text{LiOH}/\text{Li}_2\text{CO}_3$ layer with thicknesses of 10–30 nm.^[36,38] When considering the XPS penetration depth of 5–10 nm, the occurrence of Li_2O points to the predominant removal of the outer $\text{Li}_2\text{CO}_3/\text{LiOH}$ layer. This agrees with ATR-IR (Figure 1).

Taking these observations together, we conclude that a LiBFEP-enriched layer forms on the outer surface of the 0.15-HBFEP sample. The higher amount of LiBFEP and the lower $\text{Li}_2\text{CO}_3/\text{LiOH}$ content in this sample result from the reaction with the more concentrated acid solution during Li treatment. The visibility of Li_2O also points to a major removal of the top $\text{Li}_2\text{CO}_3/\text{LiOH}$ native oxide layer. Accordingly, it is probable that



Scheme 2. Proposed decomposition pathway of LiBFEP upon reaction with elemental Li. X_1, X_m indicate further decomposition products.

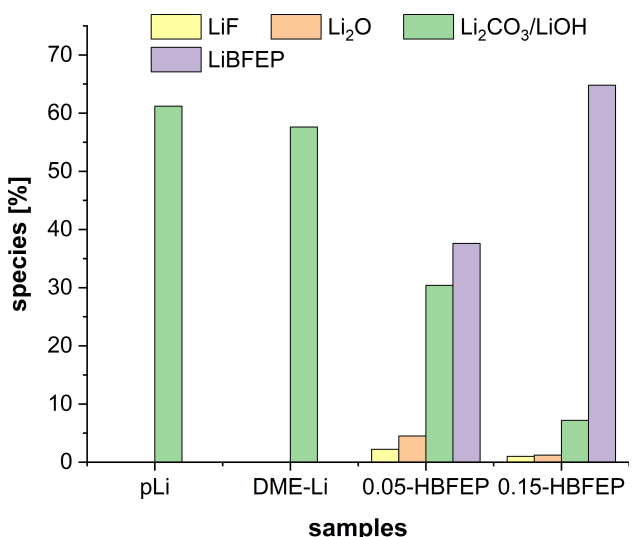


Figure 3. Representative relative amounts of Li₂O, Li₂CO₃/LiOH, LiF and LiBFEP species on the Li surfaces from XPS measurements of the different samples.

the lower LiF content in the 0.15-HBFEP sample (Figure 2d) may result from the LiBFEP predominance within the outer 5–10 nm of the surface.

SEM

In addition to the chemical characterization, scanning electron microscopy (SEM) of pLi and HBFEP-treated Li surfaces were conducted (Figure 4). The surface of pLi exhibits ridge-lines and a rather rough morphology with submicrometer-sized inhomogeneously distributed particles (Figure 4a–c). The morphology of the DME-treated Li surface (Figure S-2) is similar. The ridge-lined surface morphology is still retained in the 0.05-HBFEP sample (Figure 4d). A closer look reveals several lines crossing the whole surface of the sample. Upon magnification, a porous structure within and beside the lines becomes visible. The porous structure is formed by holes with sharp and rectangular edges (Figure 4e, f). The surface of the 0.15-HBFEP sample exhibits two different domains (Figure 4g–l) throughout the whole Li surface. One domain consists of crater-like holes and is predominant. Even there, a substructure of irregularly sized particles is visible (Figure 4i). The minor domain is rather flat. It features a similar porous morphology as the 0.05-HBFEP sample (Figure 4j–l). These crater like holes in the 0.15-HBFEP sample are most probably related to gas formation [Equations (1)–(4), (6), (7)]. On the other hand, the occurrence of holes with rectangular and sharp edges in both samples is peculiar. This morphology might be a result of etching or dissolution of a surface species with preferred crystallographic orientation, e.g., Li₂CO₃ or an expulsion of LiBFEP crystallites in the SEM vacuum chamber as a consequence of underlying solvent inclusion.

To characterize the composition of the modified Li electrodes, EDX elemental mapping analyses (Figure 5) were performed. The results for the 0.05-HBFEP sample are shown

exemplarily, while the results for the 0.15-HBFEP sample are provided in the Supporting Information (Figure S-3). A homogeneous distribution of the elements O, P, and F can be well observed on the sample surface (Figure 5b–d), which suggests a homogeneous coverage of the Li-metal surface by LiBFEP. The thickness of the layer on the 0.05-HBFEP sample has been graphically estimated to amount to $3.1 \pm 0.2 \mu\text{m}$ from the F and P EDX mappings (Figure 5g, h; cf. Supporting Information for further details).

Li–Li-symmetrical cells

After having investigated the morphological features of the deposited layer and its chemical constitution, its impact on the cyclability of Li was examined. Figure 6(a) exemplarily shows the effects of differently treated Li electrodes in Li–Li symmetrical model coin-cell tests in a voltage-time (*U*-*t*) diagram. These cell experiments simulate the plating and stripping behavior of Li during battery operation. As a model electrolyte, a 1 M LiOTf solution in TEGDME was selected (OTf = OSO₂CF₃). Furthermore, a current density of 0.1 mA cm^{-2} and an areal capacity of 0.1 mAh cm^{-2} were chosen as test parameters.^[44] Similar electrolytes are known to lead to fast battery failure in Li–Li-symmetrical cells.^[45] Hence, life-prolonging effects of the artificial SEI can be seen comparably fast with this electrolyte. Here, the true effects are revealed by the rather low current densities and areal capacities ($> 1 \text{ mA cm}^{-2}$ and $> 1 \text{ mAh cm}^{-2}$) are often used in order to evaluate the rechargeability of the Li anode with carbonate-based electrolytes.^[46] However, the 1 M LiOTf/TEGDME model electrolyte has rather limited transport properties and therefore has an impact on the overpotential. Hence, the low ionic conductivity of the TEGDME based electrolyte ($\approx 0.8 \text{ mS cm}^{-1}$)^[47] compared to LP57 ($9.0 \pm 0.1 \text{ mS cm}^{-1}$)^[48] induces a higher ohmic resistance in the cell and contributes to the overall overpotential. The ohmic resistance increases with higher current density and outweighs the life-prolonging effect of the stabilizing LiBFEP layer. Therefore, the use of higher current densities will overshadow conclusions on the stability of the LiBFEP layer here, unless the single contributions to the overpotential can be definitely separated and quantified. Considering that background knowledge and the model character of the current study, Li–Li-symmetrical cell tests with higher current were not included in the following discussion.

The battery failure in our setup is generally seen by a sudden drop of the voltage *U* to almost 0 V or its continuous increase as shown in Figure 6. The latter behavior was observed by previous authors,^[45,49] and the effect can be explained as follows: During long-term cycling of symmetrical Li/Li⁺ cells, a high amount of accumulated dead Li is formed on the electrode surface. As a result of this process the Li⁺-ion migration through the formed tortuous interphase is increasingly deteriorated, and the overall ionic mass transport from the electrolyte into the bulk Li is impeded.^[49] This effect is also claimed to be responsible for the failure of LMBs.^[50] At the

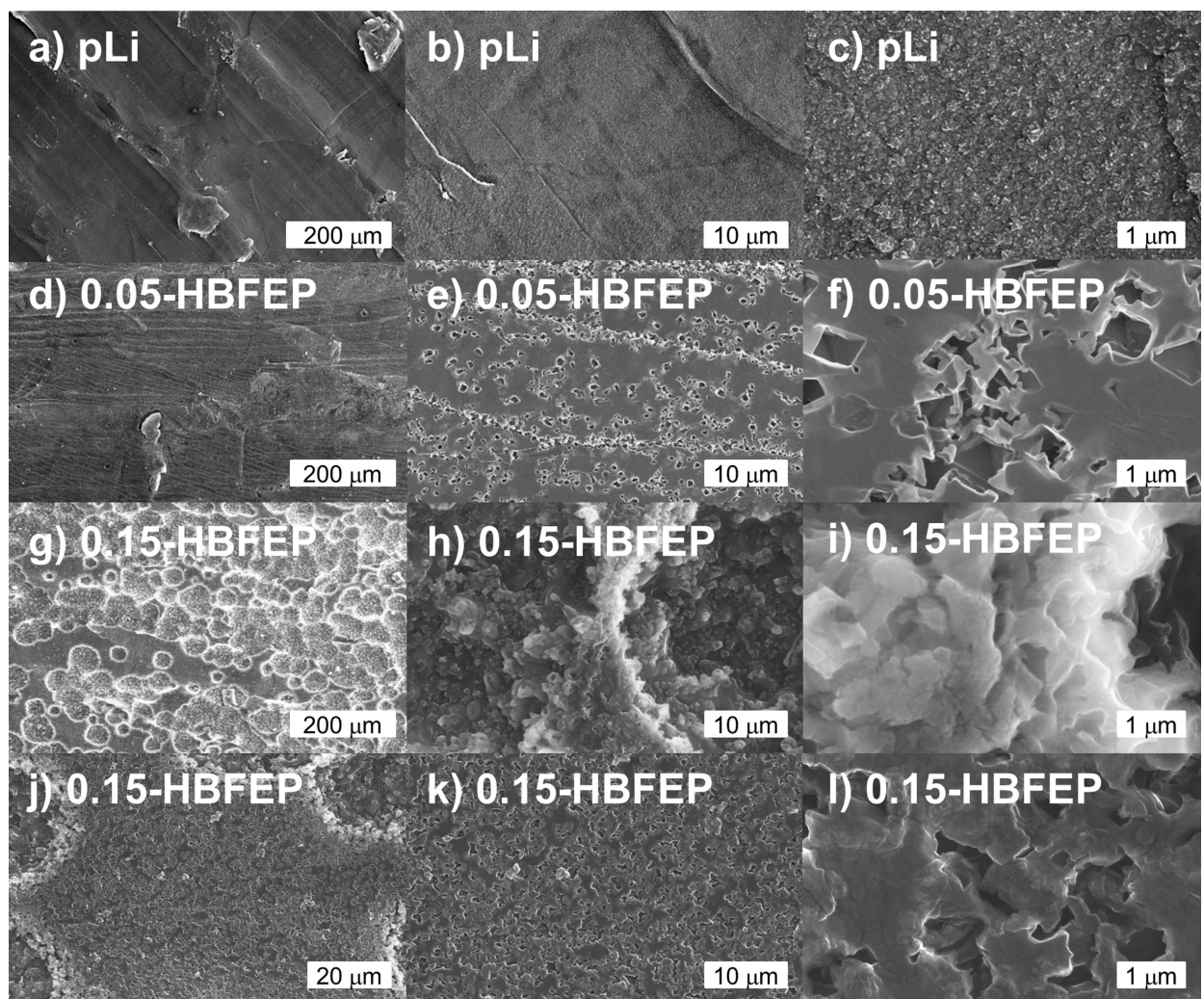


Figure 4. SEM images of the surfaces of a–c) pristine Li, d–f) 0.05-HBFEP and g–l) 0.15-HBFEP samples at different magnifications.

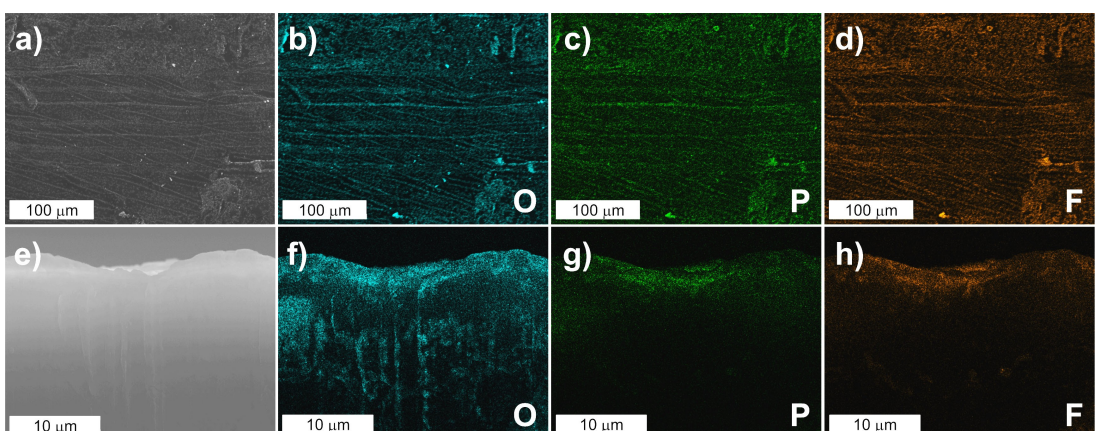


Figure 5. EDX mapping analysis of the surface (a–d) and of cross section (e–h) of a 0.05-HBFEP sample: a and e) show the micrograph of the selected areas, while b–d) and f–h) display the corresponding elemental distributions of O, P, F.

same time, the increasing depletion of the electrolyte by decomposition results in a continuous deterioration of its ion-transport properties, i.e., the ionic conductivity gradually

decreases. Both effects are assumed to be in charge of the continuous increase of U .^[49] For this manuscript, the cell lifetime, which is discussed below, refers to the cycle number

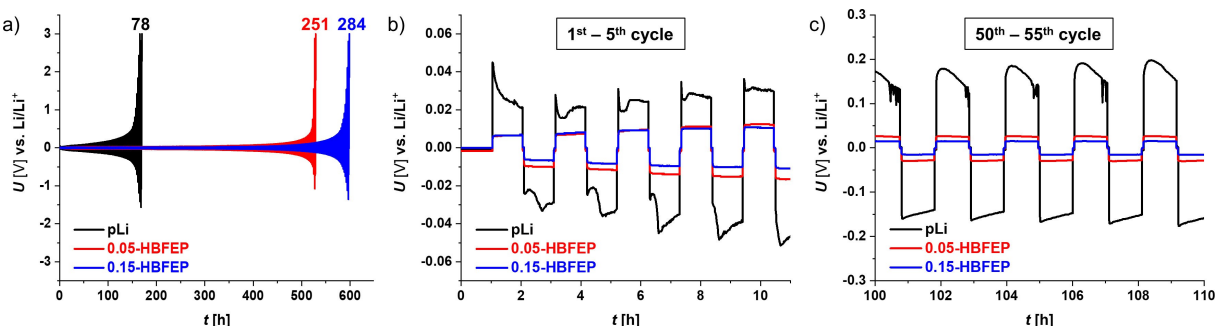


Figure 6. Voltage-time diagrams of Li–Li-symmetrical cells at 0.1 mA cm^{-2} (0.1 mAh cm^{-2}) with pristine Li (pLi) and Li treated with a 0.05 M (0.05-HBFEP) or a 0.15 M (0.15-HBFEP) HBFEP–DME solution; a) Overall course of the cell tests until the voltage cutoff of 3 V was reached. The inserted numbers above the curves correspond to the cycle lifetime; b, c) selected regions of a) illustrating the detailed evolution of the overpotentials in the investigated cells.

at which the potential reached a value of $\pm 3 \text{ V}$. For comparison, pristine Li discs (pLi) and Li discs treated with solutions of HBFEP in DME were also investigated. First, we studied the impact of the immersion time on the cell-cycle life. For this purpose, we immersed Li discs for 2, 4, and 10 min in a 0.05 M HBFEP solution (Figure S-5). An increase of the cell lifetime upon increasing the immersion time from 2 to 4 min was observed, but an extended immersion time of 10 min did not result in statistically significant effects. For the subsequent experiments, the immersion time was fixed to 4 min.

Further, a comparison of Li discs either treated with 0.05 or 0.15 M HBFEP solution in DME (0.05-HBFEP and 0.15-HBFEP, respectively) with pristine Li (pLi) was conducted. According to Figure 6a, pristine Li cells already fail after 78 cycles, while the treated Li samples 0.05-HBFEP and 0.15-HBFEP show a 3.2- and 3.6-fold prolongation of the cell lifetime to 251 and 284 cycles, respectively. To exclude that the life-prolonging effect is caused by the presence of DME only, symmetrical cells with Li treated by DME for 4 min were prepared and tested. The corresponding DME–Li symmetrical cells showed a similar behavior as the pLi cells (Figure S-6). Thus, the stabilizing effect on Li metal cycling is either attributed to the presence of the $[\text{BFEP}]^-$ anion only, or at least to the $[\text{BFEP}]^-$ anion in combination with DME molecules. Comparing the 0.05-HBFEP and 0.15-HBFEP samples, an additional improvement in the cell lifetime was observed for Li discs treated with higher concentration.

Evolution of the overpotential

The beneficial effect of the HBFEP treatment is evident from the detailed view of the voltage-time (U - t) diagrams at selected test-time periods (Figure 6b, c). Pristine Li exhibits a sharp and rather irregular evolution of the overpotential, which is related to the non-uniform Li plating/stripping during cycling of the Li metal electrode.^[45] In contrast, the U (t) evolution of the HBFEP-modified Li electrodes is rather flat, thus suggesting a smooth Li plating/stripping capability. Even at cycle numbers 50–55 (Figure 6c), in the range where the overpotential of pristine Li cells rose significantly, the values for the HBFEP-modified Li cells remained rather flat and uniform at $\pm 30 \text{ mV}$ for 0.05-HBFEP and $\pm 15 \text{ mV}$ for 0.15-HBFEP. These findings support the

formation of a favorable, protective and at the same time Li-ion conducting artificial SEI. The U (t) profiles of the 0.05-HBFEP and 0.15-HBFEP samples are quite similar. The only difference is that the overpotentials of the latter samples are slightly lower. This finding can be attributed to the thickness and morphology of the resulting layer on top of the Li surface.

Comparison to literature results – restraining the search to wet-chemical Li-anode treatments – was quite difficult, since most symmetrical cell tests were reported with carbonate-based electrolytes.^[11] Further difficulties arose due to incomplete experimental descriptions with regard to the electrolyte amount, the areal capacity, the Li anode thickness, the kind of separator, etc. Thus, only orienting comparisons can be made here. Using 1 M LiOTf in TEGDME as the electrolyte at 0.1 mA cm^{-2} current density, Liu et al. reported a 2.2-fold lifetime extension after deposition of a thermoplastic polyurethane/SiO₂ composite on Li.^[51] A 4.2-fold increase in lifetime was observed by Yu et al. with PTFE treated Li, when tested under the same conditions.^[52]

Operation principle of LIBFEP: In the following section, we propose a mechanism, which explains the life-prolonging effect of HBFEP-modified Li–Li cells. Additional single-crystal X-ray diffraction data on LiBFEP crystals grown from DME as well as mass-spectrometric experiments on LiBFEP solutions were included. As shown before, LiBFEP was identified as the main constituent of the deposited layer on top of the Li surface in the bulk phase (ATR-IR) as well as on the outer surface (XPS). Hence, we were wondering, if LiBFEP might adopt a polymeric structure on the Li surface, which retains its integrity during the operation within the cell. We addressed this question by crystallizing LiBFEP from DME by layering with *n*-pentane. The salt crystallizes as a DME adduct with the formula unit $(\text{LiBFEP})_2 \cdot \text{DME}$ (Figure 7). In the cell, the compound forms 1D chains along the crystallographic *a*-axis (Figure S-7). The chains are formed by two strings of $[\text{BFEP}]^-$ anions, which are connected by rhombic Li_2O_2 units. The single Li_2O_2 rhombs are separated by eight-membered $\text{Li}_2\text{O}_4\text{P}_2$ rings. The fourth coordination site of the Li atoms is saturated by an oxygen atom of DME. The DME molecules themselves occupy a bridging position between pairs of Li_2O_2 rhombs. Since the compound crystallizes from DME – and DME is used in the deposition process of HBFEP as well – it is reasonable that the described

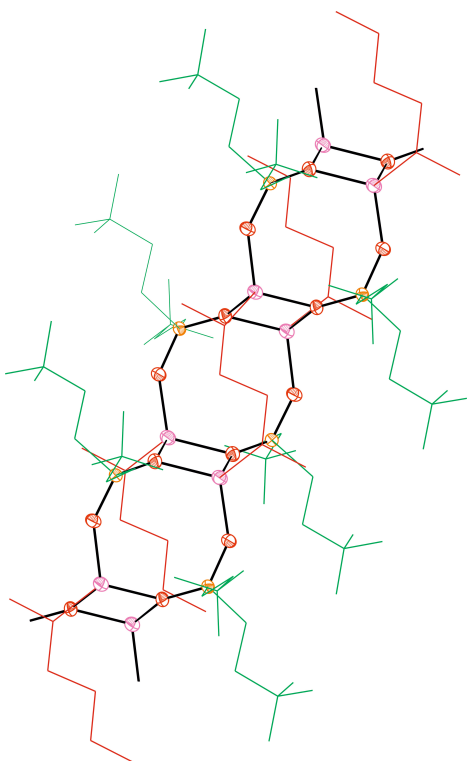


Figure 7. Molecular structure of the coordination polymer $(\text{LiBFEP})_2 \cdot \text{DME}$. Atom type colors: red = O, orange = P, purple = Li. For clarity, the bridging DME molecules are depicted as red wireframe and the two trifluoroethoxy groups bound to each phosphorous atom are provided as green wireframe. The disorder of some of the trifluoroethoxy groups is neglected.

polymeric structure might be formed on the Li-metal surface as well. As solvent-free LiBFEP can be easily obtained from diethylether solutions after synthesis,^[25] we conclude that the bridging DME molecules in the crystal structure can be easily displaced. The LiBFEP chains might be favorably attached to the Li surface by basic oxygen atoms present on the surface of bulk Li.

Electrospray ionization mass spectrometry of LiBFEP in DME in the negative-ion mode showed differently sized anionic clusters with compositions $[\text{Li}_{(n-1)}\text{[BFEP]}_n]^-$ ($n=1-7$, Figure 8 and Supporting Information).

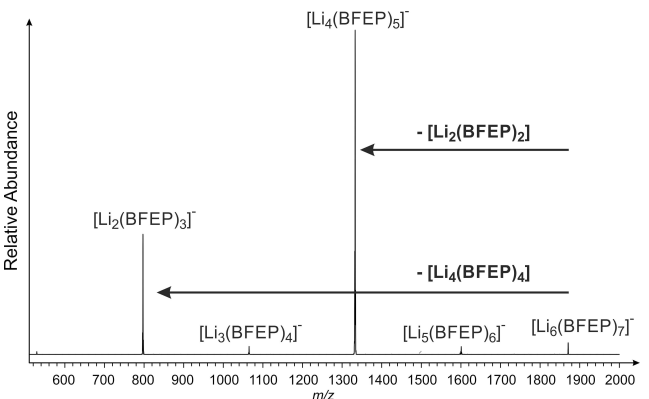
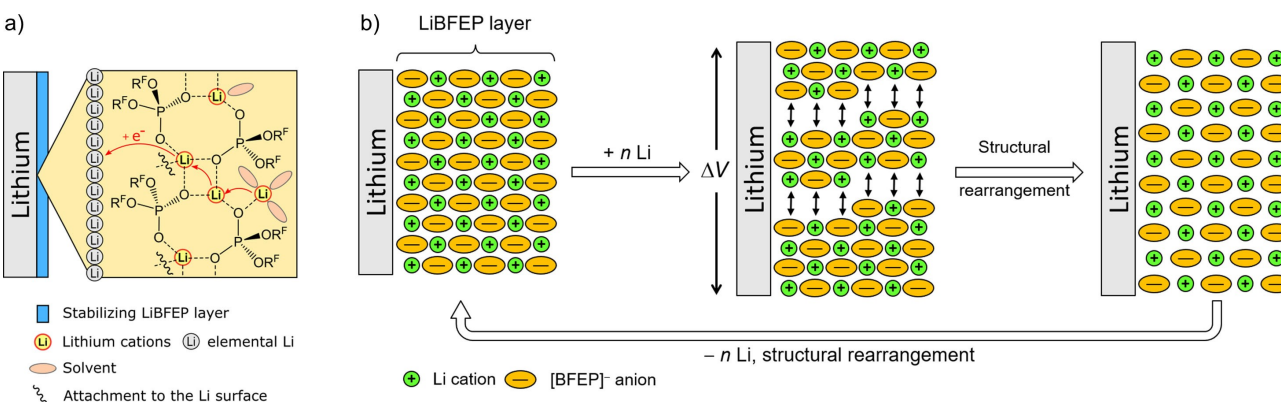


Figure 8. ESI-MS data of a LiBFEP/DME solution: collision-induced dissociation (CID) of mass-selected $[\text{Li}_6\text{[BFEP]}_7]^-$ obtained at a normalized collision energy of 20. Neutral losses of $[\text{Li}_2\text{[BFEP]}_2]$ dominate the fragmentation.

Collision-induced dissociation of these clusters results in the preferred losses of both monomeric $[\text{Li}(\text{BFEP})]$ and dimeric $[\text{Li}_2(\text{BFEP})_2]$ (see Supporting Information). With increasing size of the $[\text{Li}_{(n-1)}\text{[BFEP]}_n]^-$ clusters, the loss of $[\text{Li}_2(\text{BFEP})_2]$ dominates. The fragmentation of $[\text{Li}_6\text{[BFEP]}_7]^-$, for example, results almost exclusively in the product ions $[\text{Li}_4\text{[BFEP]}_5]^-$ and $[\text{Li}_2\text{[BFEP]}_3]^-$ (Figure 8).

Hence, the X-ray crystallographic and the mass-spectrometric observations together indicate that the polymeric structure of LiBFEP might be conserved on the Li-metal surface as well. Based on the crystallographically obtained chain structure, a 2D scheme for the Li-ion transport through the layer is proposed in Scheme 3(a). The reduction of a Li^+ ion to elemental Li at the Li-SEI interface leads to a vacancy in a Li_2O_2 rhomb. This vacancy could be filled by the adjacent Li^+ of the rhomb, thus generating a new vacancy. The latter is filled by an incoming solvated Li^+ cation, by stripping off some of its solvent molecules. The transport into the vacancy is supported by the favorable coordination of Li^+ with the O-atoms of the $[\text{BFEP}]^-$ anions.

Apart from the Li-ion conductance of the layer, its protective ability and in particular the accommodation of mechanical stress during charging is of high importance. A



Scheme 3. a) Proposed Li-ion conduction mechanism through the LiBFEP layer; b) illustration of the self-healing effect.

typical scenario is the breakage of the initial SEI during Li-plating induced by volumetric expansion of the Li electrode. The freshly generated Li surface reacts with the electrolyte, thus resulting in irreversible capacity losses and electrolyte depletion. The recurrence of these steps leads to a fast battery failure.^[11] Typical polymers might break or form cracks during expansion of the underlying surface. In the course of this process, short-lived very reactive organic radicals are formed that lead to, usually irreparable, damages. In contrast to classical polymers held by covalent bonds, however, LiBFEP is solely based on electrostatic interactions between the Li⁺ cations and the [BFEP]⁻ anions. Upon expansion of the underlying surface, only the cation-anion distance should increase. Since the underlying ions are stable entities, the cation-anion distances of the coordination polymer return to their initial state upon shrinking (Scheme 3b). If we consider the widening of the ion distances in the LiBFEP chain as a damage, the return to the original state is regarded as a repair mechanism. From that point of view, we attribute a coordination-polymer self-healing ability. At the same time, such a behavior could also be understood as self-adaptive. The hereby suggested Li-ion transport and the self-healing ability of LiBFEP are regarded as the main contributors to the observed life-prolonging effect of cells with HBFEP-treated Li. However, we would like to stress that these explanations should be regarded as helpful models only.

One concern about LiBFEP as an artificial SEI layer might be its dissolution in DME during the wet chemical treatment of Li, as well as in the electrolyte during cycling. Since we have seen the presence of LiBFEP in the ATR-IR and XPS spectra of the treated Li metal samples, a complete dissolution of the layer during the deposition process can be excluded. Instead, due to the presence of additional inorganic phases such as LiF, Li₂O, etc. we might even suggest, that the LiBFEP layer is integrated in an inorganic-organic hybrid SEI. Additional experiments showed that the solubility of LiBFEP is < 0.05 M in DME and in the TEGDME electrolyte. When considering the used HBFEP amounts, our immersion process and the electrolyte volume of 100 µL in the cell, partial dissolution of LiBFEP is in fact possible. However, the dissolution might be inhibited by the preferable polymeric chain arrangement as shown by the single-crystal structural data (Figure 7, Scheme 3) and supporting mass spectrometric studies (see text above). Nevertheless, this issue will be addressed in detail in future work.

Conclusion

In summary, we have successfully applied the fluoro-organic Brønsted acid HBFEP to modify the surface of Li metal to enhance its cyclability in rechargeable batteries. LiBFEP was deposited on the surface by immersing Li-metal discs for four minutes in a diluted (0.05 or 0.15 M) solution of HBFEP in DME. HBFEP first acts as a chemical polisher by reacting with the basic native oxide layer of the Li surface in an acid-base reaction. In the second place, the resulting reaction product LiBFEP (either alone or in combination with DME) acts as a Li-

ion conductive artificial SEI, which stabilizes the Li-metal electrode. ATR-IR and XPS measurements confirmed the predominant presence of intact LiBFEP on the Li-metal surface. The content of LiBFEP increases with the concentration of the applied HBFEP solution, while the content of basic surface species (Li₂CO₃ and LiOH) decreases at the same time. LiBFEP is deposited on Li in the form of porous layers as proven by electron microscopical studies. The 0.15-HBFEP sample even displayed two different domains throughout the surface. While the layer thickness of the 0.05-HBFEP sample has been determined to 3 µm, we expect a thicker layer for the 0.15-HBFEP sample. The lifetime of LiBFEP modified Li electrodes is three (0.05-HBFEP) to almost four (0.15-HBFEP) times higher compared to the pristine Li, as shown in Li–Li symmetrical model test cells (0.1 mA cm⁻², 1 M LiOTf in TEGDME). The compound LiBFEP is considered to be a significant and cycle-life extending constituent of the artificial SEI. The principle of operation of LiBFEP is explained by a Li-ion conduction-mechanism and the adaptive, self-healing ability of the coordination polymer.

Further work on the use of carbonate-based electrolytes, the application of higher current densities, and practical test parameter in Li-metal full-cells with TMOs as cathodes^[1c,3] is currently underway. Preliminary results with the LP57 electrolyte showed a considerable lifetime extension for HBFEP-treated Li anodes in Li–Li symmetrical cells and better capacity retention in Li–NCM111 full cells. We suppose that the use of acidic compounds forming a coordination polymer with self-healing abilities as deposition reagents on Li features a promising concept for the design of artificial SEI layers for practical rechargeable Li-metal batteries.

Experimental Section

General: All manipulations were performed in an argon filled (99.999%) glovebox (GS MEGA Line 3) with <5 ppm O₂ and <1 ppm H₂O gas residual content. Accessories for the coin cell assembly (casings, spacers, spring from Gelon LIB Group) were washed with deionized water and *iso*-propanol, dried afterwards at 80 °C for several days and stored inside the glovebox. Whatman GF/A separators (Merck, pore size 1.6 µm, 260 µm thickness) were dried and stored in a similar manner. Li discs (LTS Research Laboratories, Inc., 99.95%, Ø = 15.6 mm, 450 µm thickness) were used as received without further chemical or mechanical pretreatment.

Chemicals: The key compound *bis*-(1,1,1-trifluoroethyl)phosphoric acid was synthesized and tested for purity according to Schleep et al.^[25] 1,2-dimethoxyethane (DME, Sigma-Aldrich, 99.5% anhydrous) was stored over molecular sieves (3 Å) and filtered via a syringe filter (Chromafil RC-45/15 MS, Macherey-Nagel) prior to use. Tetraethylene glycol dimethyl ether (TEGDME, Sigma Aldrich, ≥ 99%) was distilled from CaH₂ and stored over molecular sieves. The molecular sieves were activated by heat treatment at 200 °C in vacuo (10⁻¹ mbar) for 48 h. Afterwards, they were stored in the glovebox and used as drying agent for DME and TEGDME. Li trifluoromethanesulfonate (LiOTf, Sigma Aldrich, 99.995%) was dried in high vacuo (10⁻³ mbar) at 120 °C for 3 hours. A stock solution of 1 M LiOTf and filtered TEGDME was prepared inside the glovebox. The water contents of DME, TEGDME and the electrolyte

(1 M LiOTf in TEGDME) were tested via a Karl-Fischer device (TL 7500KF M3, SI Analytics) with a Hydralan Coulomat AG titer. The values were below 10 ppm.

HBFEP treatment of Li discs: The surface treatment of Li discs with HBFEP was performed inside screw capped bottles filled with a 0.05 M or 0.15 M HBFEP solution in DME. Li discs were put inside this solution and stirred for 4 min. After that the discs were put out of the solution, dried for 15 min at each side and used for further characterization.

Electrochemical measurements: Electrochemical measurements were performed at 25 °C (inside a Binder KB 53 oven) in Li–Li symmetrical CR2032 coin cells with the following configuration: negative case, spacer (0.5 mm), Li disc, separator (Whatman GF/A) impregnated with 100 µL electrolyte (1 M LiOTf in TEGDME), Li disc, spacer (0.5 mm), spring and positive case. The additional spacer was used to fill the room inside the coin cell as much as possible. The Li discs were arranged in a way that their flat sides faced the separator. The parts were crimped the MSK-110 hydraulic crimper (MTI cooperation) at a pressure about 1000 ± 50 psi (70 ± 3 bar) for 4–6 seconds. The coin cells were connected to a LAND CT2001A multi-channel battery tester. After 1 h initial rest time the cells were charged and discharged with 0.1 mA cm^{-2} within 1 h (i.e., 0.1 mAh cm^{-2} areal capacity) with 3 min rest time in between. The measurements were stopped when a predefined voltage cut-off (here ± 3 V) was achieved. Each test was repeated 2–4 times and only one representative measurement is shown in Figure 6.

Characterization techniques: Scanning electron microscopical (SEM) measurements were performed with the FEI Scios 2 HiVac device at room temperature. The samples were cut and mounted on the sample holder inside the glovebox. During the transfer of the sample into the SEM chamber a short contact with the ambient atmosphere could not be avoided. An acceleration voltage of 20 kV and an Everhart-Thornley detector (ETD) in the secondary electron (SE) mode were used. An EDAX Octane Elite system was used for the EDX measurements (20 kV acceleration voltage). ATR-IR spectra were recorded inside the glovebox with a Bruker alpha Fourier transform IR spectrometer using a diamond ATR unit. The samples were slightly pressed with the stamp to ensure sufficient contact to the ATR unit. No ATR and no baseline corrections were performed to exclude artefacts. Peak picking was performed with Origin. XPS spectra were acquired using a Thermo Scientific K-alpha spectrometer. The samples were analyzed using a microfocused, monochromated Al K_{α} X-ray source (1486.6 eV, 400 µm spot size). XPS spectra were recorded with a concentric hemispherical analyzer at a pass energy of 50 eV and fit with one or more Voigt profiles (binding energy uncertainty: ± 0.2 eV). Scofield sensitivity factors^[53] were applied for quantification using the Avantage software package. All spectra were referenced to the C 1s peak (C–C/C–H) at 285.0 eV binding energy controlled by means of the photoelectron peaks of metallic Cu, Ag, and Au, respectively. The fluorine (F1s) spectra were done at the beginning and after each resolution analysis, to check for absence of any sample degradation under irradiation.

Single-crystal X-ray diffraction: Single-crystal X-ray data were collected on a Bruker D8 VENTURE dual wavelength Mo/Cu three-circle diffractometer both with a microfocus sealed X-ray tube using Incoatec mirror optics as a monochromator. The diffractometer is equipped with an Oxford Cryostream 800 low-temperature device, and Mo K_{α} radiation ($\lambda = 0.71073 \text{ \AA}$) was used for the measurement. Single crystals of $(\text{LiBFEP})_2 \cdot \text{DME}$ were obtained at room temperature from a saturated solution of LiBFEP in dimethoxyethane by layering with *n*-pentane. The crystals were mounted at room temperature in mineral oil and were shock-cooled to 100.0 K on the diffractometer. Data were integrated with SAINT,^[54] and a multi-scan absorption-correction using SADABS-2016/2 was

applied.^[55] The structures were solved by direct methods using SHELXT 2018/2^[56] and refined by full-matrix least-squares methods against F^2 by SHELXL-2018/3^[57] employing shelXle (Revision 1334).^[58] All non-hydrogen atoms were refined with anisotropic displacement parameters. The hydrogen atoms were refined isotropically on calculated positions using a riding model with their U_{iso} values constrained to 1.5 times the U_{eq} of their pivot atoms for terminal sp^3 carbon atoms and 1.2 times for all other carbon atoms. Disordered moieties were refined using bond-length restraints and displacement-parameter restraints. Some parts of the disorder model were introduced by the program DSR.^[59] Crystallographic data for the structure reported in this paper have been deposited with the Cambridge Crystallographic Data Centre. 2110842 contains the supplementary crystallographic data for this paper. These data are provided free of charge by the joint Cambridge Crystallographic Data Centre and Fachinformationszentrum Karlsruhe Access Structures service.

Mass spectrometry: The mass-spectrometric experiments were performed with a Thermo-Fischer LTQ XL linear ion-trap mass-spectrometer equipped with an electrospray-ionization (ESI) source. Mass spectra of LiBFEP were obtained by electrospray ionization from a millimolar solution in dimethoxyethane. The Capillary Temperature was set to 150 °C to avoid fragmentation of the ions on their way to the analyzer. Nitrogen was used as a Sheath, Sweep, and Auxiliary Gas at flow rates to 0, 10, and 2, respectively (given in arbitrary units). The Source Voltage was set to 3.5 kV, the Tube Lens Voltage was adjusted to 80 V, and the Capillary Voltage was set to 25 V. The identity of the ions was confirmed by comparison of the relative signal intensities with simulated isotope patterns, complemented by collision-induced dissociation (CID). In the CID experiments, helium served as collision gas. The supplied collision energy was adjusted by varying the Normalized Collision Energy (NCE) between 0 and 40. Note that this value is given in arbitrary units, and a conversion to an E_{lab} scale is difficult. Therefore, we refrain from a more detailed discussion of absolute collision energies.

Acknowledgements

The authors acknowledge support by the Vector Stiftung through the project "LIM-MOBIL". The authors appreciate funding support from Alexander von Humboldt Foundation. The Freiburg Center for Interactive Materials and Bioinspired Technologies (FIT) is acknowledged for providing the necessary infrastructure. We thank the Karlsruhe Nano Micro Facility (KNMF) for providing XPS measurement facilities. W.B. expresses his gratitude to his previous hosts Dr. Severin Vierrath, Dr. Mathias Breitwieser, and Prof. Dr. Zengerle (Department of Microsystems Engineering – IMTEK) as well as the current host Prof. Dr. Hans-Martin Henning (Department of Sustainable Systems Engineering – INATECH) for the necessary support during the project. Venkata Aditya Kiran Adiraju and Prof. Dr. Brett Lucht (University of Rhode Island) are acknowledged for providing additional reference ATR-IR spectra for proper assignments, shown in Table S1 in the Supporting Information. Open Access funding enabled and organized by Projekt DEAL.

Conflict of Interest

The authors declare no conflict of interest.

Data Availability Statement

The data that support the findings of this study are available from the corresponding author upon reasonable request.

Keywords: artificial solid electrolyte interphase · electrochemistry · inorganic coordination polymer · Li metal batteries · surface analysis

- [1] a) M. Ue, K. Sakaushi, K. Uosaki, *Mater. Horiz.* **2020**, *7*, 1937; b) J. Betz, G. Bieker, P. Meister, T. Placke, M. Winter, R. Schmuck, *Adv. Energy Mater.* **2019**, *9*, 1803170; c) J. Liu, Z. Bao, Y. Cui, E. J. Dufek, J. B. Goodenough, P. Khalifah, Q. Li, B. Y. Liaw, P. Liu, A. Manthiram, Y. S. Meng, V. R. Subramanian, M. F. Toney, V. V. Viswanathan, M. S. Whittingham, J. Xiao, W. Xu, J. Yang, X.-Q. Yang, J.-G. Zhang, *Nat. Energy* **2019**, *4*, 180; d) J. W. Choi, D. Aurbach, *Nat. Rev. Mater.* **2016**, *1*, 16013; e) E. J. Berg, C. Villevieille, D. Streich, S. Trabesinger, P. Novák, *J. Electrochem. Soc.* **2015**, *162*, A2468.
- [2] C. Niu, H. Lee, S. Chen, Q. Li, J. Du, W. Xu, J.-G. Zhang, M. S. Whittingham, J. Xiao, J. Liu, *Nat. Energy* **2019**, *4*, 551.
- [3] C. Niu, H. Pan, W. Xu, J. Xiao, J.-G. Zhang, L. Luo, C. Wang, D. Mei, J. Meng, X. Wang, Z. Liu, L. Mai, J. Liu, *Nat. Nanotechnol.* **2019**, *14*, 594.
- [4] Y. Gao, M. Guo, K. Yuan, C. Shen, Z. Ren, K. Zhang, H. Zhao, F. Qiao, J. Gu, Y. Qi, K. Xi, B. Wei, *Adv. Energy Mater.* **2020**, *10*, 1903362.
- [5] Y. Qiao, H. Deng, P. He, H. Zhou, *Joule* **2020**, *4*, 1445.
- [6] a) Specification data sheet for the Licerion® Technology (<https://sionpower.com/products/>), requested from SionPower on September 9, 2020; b) Y. Mikhaylik, I. Kovalev, C. Scordilis-Kelley, L. Liao, M. Laramie, U. Schoop, T. Kelley, *Meet. Abstr.* **2018**, MA2018-01, 302.
- [7] Technical Report, Data Week 2021, Solid Energy Systems (SES), (<https://ses.ai/investors/>); data retrieved on October 25, 2021.
- [8] A. Thielmann, M. Wietschel, S. Funke, A. Grimm, T. Hettesheimer, S. Langkau, A. Loibl, C. Moll, C. Neef, P. Plötz, L. Sievers, L. T. Espinoza, J. Edler, *Batterien für Elektroautos: Faktencheck und Handlungsbedarf*, Karlsruhe, **2020**.
- [9] Specification data sheet for OXIS—Li—S-Ultra-Light-Cell (<https://oxisenergy.com/products/>), last accessed on October 15, 2021.
- [10] D. Lin, Y. Liu, Y. Cui, *Nat. Nanotechnol.* **2017**, *12*, 194.
- [11] X.-B. Cheng, R. Zhang, C.-Z. Zhao, Q. Zhang, *Chem. Rev.* **2017**, *117*, 10403.
- [12] K. Zhang, G.-H. Lee, M. Park, W. Li, Y.-M. Kang, *Adv. Energy Mater.* **2016**, *6*, 1600811.
- [13] J. Lang, L. Qi, Y. Luo, H. Wu, *Energy Storage Mater.* **2017**, *7*, 115.
- [14] H. Yang, C. Guo, A. Naveed, J. Lei, J. Yang, Y. Nuli, J. Wang, *Energy Storage Mater.* **2018**, *14*, 199.
- [15] J. H. Um, K. Kim, J. Park, Y.-E. Sung, S.-H. Yu, *J. Mater. Chem. A* **2020**, *8*, 13874.
- [16] N. Delaporte, Y. Wang, K. Zaghib, *Front. Mater.* **2019**, *6*, 267.
- [17] R. Xu, X.-B. Cheng, C. Yan, X.-Q. Zhang, Y. Xiao, C.-Z. Zhao, J.-Q. Huang, Q. Zhang, *Matter* **2019**, *1*, 317.
- [18] Z. Yu, Y. Cui, Z. Bao, *Cell Reports Physical Science* **2020**, *1*, 100119.
- [19] H. Zhou, S. Yu, H. Liu, P. Liu, *J. Power Sources* **2020**, *450*, 227632.
- [20] M. Winter, *Z. Phys. Chem.* **2009**, *223*, 1395.
- [21] M. Gauthier, T. J. Carney, A. Grimaud, L. Giordano, N. Pour, H.-H. Chang, D. P. Fenning, S. F. Lux, O. Paschos, C. Bauer, F. Maglia, S. Lupart, P. Lamp, Y. Shao-Horn, *J. Phys. Chem. Lett.* **2015**, *6*, 4653.
- [22] a) Y. J. Zhang, W. Wang, H. Tang, W. Q. Bai, X. Ge, X. L. Wang, C. D. Gu, J. P. Tu, *J. Power Sources* **2015**, *277*, 304; b) G. Ma, Z. Wen, M. Wu, C. Shen, Q. Wang, J. Jin, X. Wu, *Chem. Commun.* **2014**, *50*, 14209; c) H. Chen, A. Pei, D. Lin, J. Xie, A. Yang, J. Xu, K. Lin, J. Wang, H. Wang, F. Shi, D. Boyle, Y. Cui, *Adv. Energy Mater.* **2019**, *9*, 1900858; d) J. Zhao, L. Liao, F. Shi, T. Lei, G. Chen, A. Pei, J. Sun, K. Yan, G. Zhou, J. Xie, C. Liu, Y. Li, Z. Liang, Z. Bao, Y. Cui, *J. Am. Chem. Soc.* **2017**, *139*, 11550.
- [23] a) G. A. Umeda, E. Menke, M. Richard, K. L. Stamm, F. Wudl, B. Dunn, *J. Mater. Chem.* **2011**, *21*, 1593; b) S. Neuhold, D. J. Schroeder, J. T. Vaughey, *J. Power Sources* **2012**, *206*, 295; c) M. Wu, Z. Wen, J. Jin, B. V. R. Chowdari, *ACS Appl. Mater. Interfaces* **2016**, *8*, 16386; d) A. Basile, A. I. Bhatt, A. P. O'Mullane, *Nat. Commun.* **2016**, *7*, 11794; e) L. Lin, F. Liang, K. Zhang, H. Mao, J. Yang, Y. Qian, *J. Mater. Chem. A* **2018**, *6*, 15859; f) C. Yan, X.-B. Cheng, Y. Tian, X. Chen, X.-Q. Zhang, W.-J. Li, J.-Q. Huang, Q. Zhang, *Adv. Mater.* **2018**, *30*, 1707629.
- [24] a) M. Wu, J. Jin, Z. Wen, *RSC Adv.* **2016**, *6*, 40270; b) X. Liang, Q. Pang, I. R. Kochetkov, M. S. Sempere, H. Huang, X. Sun, L. F. Nazar, *Nat. Energy* **2017**, *2*, 17119; c) M. Bai, K. Xie, K. Yuan, K. Zhang, N. Li, C. Shen, Y. Lai, R. Vajtai, P. Ajayan, B. Wei, *Adv. Mater.* **2018**, *30*, 1801213; d) Y. Lu, S. Gu, X. Hong, K. Rui, X. Huang, J. Jin, C. Chen, J. Yang, Z. Wen, *Energy Storage Mater.* **2018**, *11*, 16; e) J. Bobnar, M. Lozinšek, G. Kapun, C. Njel, R. Dedryvère, B. Genorio, R. Dominko, *Sci. Rep.* **2018**, *8*, 5819; f) S. Li, Q. Liu, X. Wang, Q. Wu, L. Fan, W. Zhang, Z. Shen, L. Wang, M. Ling, Y. Lu, *ACS Materials Lett.* **2020**, *2*, 1; g) Q. Li, F.-L. Zeng, Y.-P. Guan, Z.-Q. Jin, Y.-Q. Huang, M. Yao, W.-K. Wang, A.-B. Wang, *Energy Storage Mater.* **2018**, *13*, 151; h) J. Luo, C.-C. Fang, N.-L. Wu, *Adv. Energy Mater.* **2018**, *8*, 1701482; i) Y. Liu, D. Lin, P. Y. Yuen, K. Liu, J. Xie, R. H. Dauskardt, Y. Cui, *Adv. Mater.* **2017**, *29*, 1605531.
- [25] M. Schleep, S. Reininger, P. Eiden, P. Klose, C. Schulz, H. Scherer, S. Laule, S. Bodendorfer, M. Schmidt, A. Garsuch, I. Krossing, *ChemElectroChem* **2016**, *3*, 774.
- [26] M. S. Milien, H. Beyer, W. Beichel, P. Klose, H. A. Gasteiger, B. L. Lucht, I. Krossing, *J. Electrochem. Soc.* **2018**, *165*, A2569.
- [27] S. Wang, M. W. Urban, *Nat. Rev. Mater.* **2020**, *5*, 562.
- [28] N.-W. Li, Y. Shi, Y.-X. Yin, X.-X. Zeng, J.-Y. Li, C.-J. Li, L.-J. Wan, R. Wen, Y.-G. Guo, *Angew. Chem. Int. Ed.* **2018**, *57*, 1505.
- [29] W. Tang, X. Yin, Z. Chen, W. Fu, K. P. Loh, G. W. Zheng, *Energy Storage Mater.* **2018**, *14*, 289.
- [30] W. Jia, Q. Wang, J. Yang, C. Fan, L. Wang, J. Li, *ACS Appl. Mater. Interfaces* **2017**, *9*, 7068.
- [31] N.-W. Li, Y.-X. Yin, C.-P. Yang, Y.-G. Guo, *Adv. Mater.* **2016**, *28*, 1853.
- [32] Y. Nan, S. Li, M. Zhu, B. Li, S. Yang, *ACS Appl. Mater. Interfaces* **2019**, *11*, 28878.
- [33] F. Ding, W. Xu, X. Chen, J. Zhang, Y. Shao, M. H. Engelhard, Y. Zhang, T. A. Blake, G. L. Graff, X. Liu, J. G. Zhang, *J. Phys. Chem. C* **2014**, *118*, 4043.
- [34] J. Xu, C. Ding, P. Chen, L. Tan, C. Chen, J. Fu, *Appl. Phys. Rev.* **2020**, *7*, 31304.
- [35] D. Aurbach, M. L. Daroux, P. W. Faguy, E. Yeager, *J. Electrochem. Soc.* **1988**, *135*, 1863.
- [36] a) K. Kanamura, H. Tamura, S. Shiraishi, Z.-i. Takehara, *J. Electrochem. Soc.* **1995**, *142*, 340; b) K.-i. Morigaki, A. Ohta, *J. Power Sources* **1998**, *76*, 159; c) M. L. Meyerson, J. K. Sheavly, A. Dolocan, M. P. Griffin, A. H. Pandit, R. Rodriguez, R. M. Stephens, D. A. Vandenberg, A. Heller, C. B. Mullins, *J. Mater. Chem. A* **2019**, *7*, 14882; d) S.-K. Otto, Y. Moryson, T. Krauskopf, K. Peppler, J. Sann, J. Janek, A. Henss, *Chem. Mater.* **2021**, *33*, 859.
- [37] M. Hesse, H. Meier, B. Zeh *Spektroskopische Methoden in der organischen Chemie*, 7th edition, Thieme, Stuttgart, New-York, **2005**, pp. 33–72.
- [38] C. Naudin, J. L. Bruneel, M. Chami, B. Desbat, J. Grondin, J. C. Lassègues, L. Servant, *J. Power Sources* **2003**, *124*, 518.
- [39] a) D. Aurbach, Y. Gofer, J. Langsam, *J. Electrochem. Soc.* **1989**, *136*, 3198; b) D. Aurbach, D. L. Daroux, P. W. Faguy, E. Yeager, *J. Electrochem. Soc.* **1988**, *135*, 1863.
- [40] J. Becking, A. Gröbmeyer, M. Kolek, U. Rodehorst, S. Schulze, M. Winter, P. Bieker, M. C. Stan, *Adv. Mater. Interfaces* **2017**, *4*, 1700166.
- [41] N. Pavlin, S. Hribernik, G. Kapun, S. D. Talian, C. Njel, R. Dedryvère, R. Dominko, *J. Electrochem. Soc.* **2019**, *166*, A5237.
- [42] S. Leroy, H. Martinez, R. Dedryvère, D. Lemordant, D. Gonbeau, *Appl. Surf. Sci.* **2007**, *253*, 4895.
- [43] G. G. Eshetu, X. Judez, C. Li, M. Martinez-Ibañez, I. Gracia, O. Bondarchuk, J. Carrasco, L. M. Rodriguez-Martinez, H. Zhang, M. Armand, *J. Am. Chem. Soc.* **2018**, *140*, 9921.
- [44] The electrolyte was chosen with the prospect to apply such stabilized Li-metal anodes in Li—O₂ battery cells by one of us. L. Liu, unpublished results.
- [45] G. Bieker, M. Winter, P. Bieker, *Phys. Chem. Chem. Phys.* **2015**, *17*, 8670.
- [46] E. Markevich, G. Salitra, F. Chesneau, M. Schmidt, D. Aurbach, *ACS Energy Lett.* **2017**, *2*, 1321.
- [47] G. A. Elia, J.-B. Park, Y.-K. Sun, B. Scrosati, J. Hassoun, *ChemElectroChem* **2014**, *1*, 47.
- [48] J. Landesfeind, H. A. Gasteiger, *J. Electrochem. Soc.* **2019**, *166*(14) A3079.

- [49] K.-H. Chen, K. N. Wood, E. Kazyak, W. S. LePage, A. L. Davis, A. J. Sanchez, N. P. Dasgupta, *J. Mater. Chem. A* **2017**, *5*, 11671.
- [50] D. Lu, Y. Shao, T. Lozano, W. D. Bennett, G. L. Graff, B. Polzin, J. Zhang, M. H. Engelhard, N. T. Saenz, W. A. Henderson, P. Bhattacharya, J. Liu, J. Xiao, *Adv. Energy Mater.* **2015**, *5*, 1400993.
- [51] T. Liu, X.-L. Feng, X. Jin, M.-Z. Shao, Y.-T. Su, Y. Zhang, X.-B. Zhang, *Angew. Chem. Int. Ed.* **2019**, *58*, 18240.
- [52] Y. Yu, G. Huang, J.-Z. Wang, K. Li, J.-L. Ma, X.-B. Zhang, *Adv. Mater.* **2020**, *32*, 2004157.
- [53] J. H. Scofield, *J. Electron Spectrosc. Relat. Phenom.* **1976**, *8*, 129.
- [54] SAINT V8.38A, Bruker AXS, Madison, Wisconsin, USA, 2015.
- [55] L. Krause, R. Herbst-Irmer, G. M. Sheldrick, D. Stalke, *J. Appl. Crystallogr.* **2015**, *48*, 3.
- [56] G. M. Sheldrick, *Acta Crystallogr. Sect. A: Found. Crystallogr.* **2015**, *71*, 3.
- [57] G. M. Sheldrick, *Acta Crystallogr. Sect. C: Cryst. Struct. Commun.* **2015**, *71*, 3.
- [58] C. B. Hübschle, G. M. Sheldrick, B. Dittrich, *J. Appl. Crystallogr.* **2011**, *44*, 1281.
- [59] a) D. Kratzert, J. J. Holstein, I. Krossing, *J. Appl. Crystallogr.* **2015**, *48*, 933;
b) D. Kratzert, I. Krossing, *J. Appl. Crystallogr.* **2018**, *51*, 928.

Manuscript received: November 15, 2021
Version of record online: December 16, 2021